

Glycidyl methacrylate-modified gum arabic mediated graphene exfoliation and its use for enhancing mechanical performance of hydrogel



Jinchen Fan, Zixing Shi*, Jialiang Wang, Jie Yin

School of Chemistry and Chemical Engineering, State Key Laboratory for Metal Matrix Composite Materials, Shanghai Jiao Tong University, 200240 Shanghai, People's Republic of China

ARTICLE INFO

Article history:

Received 30 December 2012

Received in revised form

20 May 2013

Accepted 25 May 2013

Available online 4 June 2013

Keywords:

Gum arabic

Graphene

Hydrogel

ABSTRACT

Chemically-modified gum arabic with glycidyl methacrylate was used for liquid-phase direct exfoliation of graphite. Using this technique, glycidyl methacrylate-modified gum arabic-functionalized graphene flakes can be easily obtained by centrifugal separation after sonication. It was demonstrated by transmission electron microscopy, atomic force microscopy, Fourier transform infrared spectroscopy, X-ray diffraction, Raman spectroscopy and thermogravimetric analysis. The functionalized graphene flakes, coupled with vinyl groups coming from the glycidyl methacrylate-modified gum arabic, were introduced into a poly (acrylic acid) hydrogel to improve its mechanical property. Compared to poly (acrylic acid) hydrogel, the compressive strength and elastic modulus of the graphene/poly (acrylic acid) composite hydrogel with 5 wt% of functionalized graphene flakes reach ~ 49.2 and ~ 66.9 kPa, increased by $\sim 846.1\%$ and $\sim 243.7\%$, respectively.

© 2013 Elsevier Ltd. All rights reserved.

1. Introduction

Hydrogel, formed by cross-linked hydrophilic polymer chains, can swell extensively in large amounts of water without dissolution and maintain its three-dimensional network structure [1]. It attracted a great deal of attention in drug delivery system (DDS), biomedical and tissue engineering, *etc.* [2,3]. However, these applications are often limited by the poor mechanical properties of conventional chemical cross-linked hydrogel [4]. The industrial and biomedical applications of hydrogel often require the hydrogels with high mechanical properties [5].

Recently, graphene has attracted a great deal of attention due to its fascinating properties such as thermal conductivity, mechanical property and giant electronic transport property [6–8]. It can be produced by mechanical exfoliation, chemical vapour deposition and chemical reduction of exfoliated graphite oxide, *etc.* For graphite oxide, there are significant quantities of oxygen-containing groups on the basal plane and edges of the graphite [9]. Owing to the oxygen-containing groups, graphite oxide can be exfoliated to form aqueous colloidal suspensions of single-layer graphene oxide (GO)

by sonication [10]. Afterwards, GO was introduced into hydrogel for enhancing the mechanical properties of hydrogel. Shen et al. introduced GO into poly(acrylic acid) (PAA) hydrogels to modify their mechanical properties [11]. After introduction of GO, the ductility and strength of the hydrogel were greatly improved. Similarly, the tough and highly stretchable polyacrylamide (PAM)/GO composite hydrogel was synthesized by free radical polymerization [12].

GO is an insulator rather than a semi-metal and is conceptually different from graphene [13,14]. The structural defects, such as wrinkling, crumpling or atomic vacancies, which are introduced into the basal plane of GO during the extensive oxidation of graphite [15–17]. Although the functional groups of GO can be removed by reduction, large defect populations are continue to disrupt the efficiency of reinforcement for polymer composites [18,19]. On the bright side, graphene flakes can be produced by direct exfoliation of pristine graphite in liquid solution, such as N-methyl-pyrrolidone (NMP) and surfactant-water solution [20–24]. Among of these solutions, surfactant-water solution is considered to be more effective for liquid-phase exfoliation in high throughput of graphene flakes [25]. It is worth noting that the surfactant can be coated on the surface of graphene flake by physical absorption after exfoliation in surfactant-water solution [23,25]. In other words, the process can be considered to be the direct route for

* Corresponding author. Tel.: +86 21 54743268; fax: +86 21 54747445.
E-mail address: zxshi@sjtu.edu.cn (Z. Shi).

functionalization of graphene flakes. Thus, when the functional surfactant was used for exfoliation, it is easy for fabricating the graphene-based composites in further applications [26].

Gum arabic (GA), a kind of natural amphiphilic surfactant, is widely used as an emulsifier in the encapsulation of flavour oils for dried food and the manufacture of soft drinks [27]. After addition of GA, the surface tension of water can be obviously reduced due to significant surface activity [28]. In our previous study, GA was used for production of GA-functionalized graphene flakes (GAGS). The GAGS were further applied in synthesizing GAGS/Ag hybrids for surface enhanced Raman spectroscopy (SERS) [29].

Due to its biodegradability, biocompatibility and non-toxicity, GA has attracted extensive interest in applications of hydrogel [30]. However, it was observed that GA is not possible to form hydrogel from this raw material. Chemically modification of GA by reaction with glycidyl methacrylate (GMA) was considered as effective way to overcome this problem. After reaction, GA was modified by GMA with introduction of vinyl groups in the polysaccharide structure of GA. It allowed performing polymerization reaction with hydrophilic vinyl monomers [31].

Based on above consideration, GMA-GA was used for liquid-phase exfoliation of graphite. After exfoliation, the GMA-GA-functionalized graphene flakes (GMGS) were obtained by centrifugal separation. The GMGS were introduced into a poly (acrylic acid) hydrogel to improve its mechanical properties.

2. Experimental

2.1. Materials

GA ($M_w = 220\,000\text{--}300,000$ Da) and GMA were purchased from Adamas Reagent Co., Ltd. Graphite powder (100 meshes, 99.9995%) was obtained from Alfa-Aesar Co., Ltd. AA, ammonium persulfate (APS), tetramethylethylenediamine (TEMED) and N, N'-methylenebisacrylamide (BIS) were supplied by Sinopharm Co., Ltd. All other reagents were at least of analytical reagent grade and used without further purification.

2.2. Synthesis of GMA-GA

GMA-GA was synthesized by reported method [31]. 20.0 g of GA was first dissolved into the mixed aqueous-dimethylsulfoxide (DMSO) solution (50.7 mL deionized (DI) water, 129 mL DMSO). Successively, 0.127 mmol TEMED and 75.2 mmol GMA were added. The resulting mixture solution was stirred at 50 °C for 72 h. The GMA-GA was purified by precipitation of the resulting mixture solution in ethanol and re-mixed in water. Afterwards, GMA-GA were dissolved in DI water and lyophilized in a freeze-dry system for 1 week to remove water completely. Fourier transform infrared (FTIR) spectroscopy and Proton nuclear magnetic resonance (^1H NMR) spectroscopy analyses were used to characterize the GMA-GA (Supplementary data).

2.3. Preparation of GMGS

GMGS were prepared by liquid-phase exfoliation of pristine graphite with sonication in KQ-218 ultrasonicator (Shumei, China). In brief, desired amount of pristine graphite was added into GMA-GA aqueous solution, followed with sonication of 5 h in an ice-water bath. After sonication, the dispersions were centrifuged at 4000 rpm for 30 min to sediment un-exfoliated graphite particles or thick graphite flakes, and GMA-GA-stabilized graphene flakes aqueous dispersions were obtained by collecting the top supernatants. Then, GMGS were repeatedly separated and washed from the top supernatants by centrifuged at 15 000 rpm for 30 min. Finally,

the obtained GMGS were lyophilized in a freeze-dry system to remove water completely.

2.4. Fabrication of GMGS/PAA composite hydrogel

GMGS were first dispersed in 10 mL of DI water with sonication of 30 min. Next, AA (1.0 g), BIS (0.02 g) and APS (0.01 g) were added into GMGS aqueous dispersion at 0 °C as initial solution for hydrogel formation. Then, the initial solution was transferred into the glass tube (inner diameter: 15 mm and 240 mm length) and reacted at 80 °C for 2 h. After reaction, the hydrogel, in its cylindrical form, was taken out of the glass tube and immersed into DI water. The water was renewed every 8 h for 72 h, after which the hydrogel were lyophilized. The hydrogel were expressed as GMGS/PAA n hydrogel, where n stand for the amounts of GMGS (n wt% against of AA monomer).

2.5. Instruments and characterizations

FTIR spectra were recorded on a Perkin-Elmer Paragon 1000 PC spectrometer. ^1H NMR spectra were obtained on a Varian Mercury Plus-400 nuclear magnetic resonance spectrometer (400 MHz) at room temperature using D_2O as deuterated solvent. X-ray powder diffraction (XRD) patterns were recorded on a D/max-2200/PC (Japan Rigaku Corp.) using $\text{CuK}\alpha$ radiation ($\lambda = 1.5418$ Å). Raman spectra were taken on a Bruker Optics Senterra R200-L dispersive Raman micro-scope at an excitation wavelength of 532 nm. Thermogravimetric analysis (TGA) was performed in the air atmosphere with a Perkin-Elmer TGA 2050 instrument at a heating rate of 20 °C/min. Ultraviolet visible (UV-Vis) absorption spectra of were recorded by UV-2550 spectrophotometer (Shimadzu, Japan). Atomic Force Microscope (AFM) images were obtained by digital E-Sweep Atomic Force Microscope in tapping mode. The morphologies were obtained by using transmission electron microscopy (TEM) (JEOL2100F). The three-dimension network structures of hydrogels were characterized by scanning electron microscope (SEM) (JSM-7401F).

2.6. Swelling ratio of hydrogel

The swelling ratio (SR) of hydrogel was determined by immersing the dry hydrogel into aqueous solution with desired pH in sealed containers at room temperature. After regular periods of time, the hydrogel were taken out from the aqueous solution, after the removal of excess surface water with a filter paper, weighed, and returned to the previous container until reached the equilibrium swelling state. The SR is calculated from the equation: $\text{SR} = (W_s - W_d)/W_d$, where W_s and W_d represent the weights of the swollen and dry-state samples, respectively [32]. The pH values of

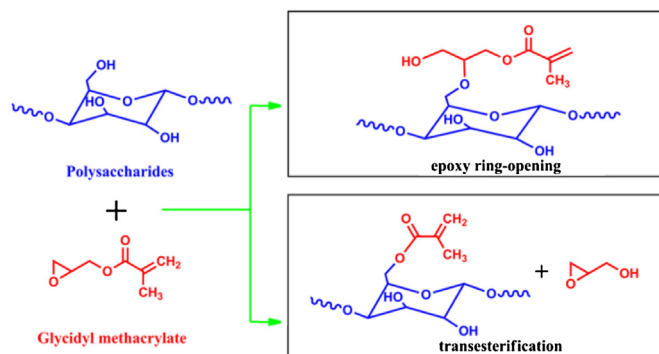


Fig. 1. Schematic drawing of the chemical modification of GA.

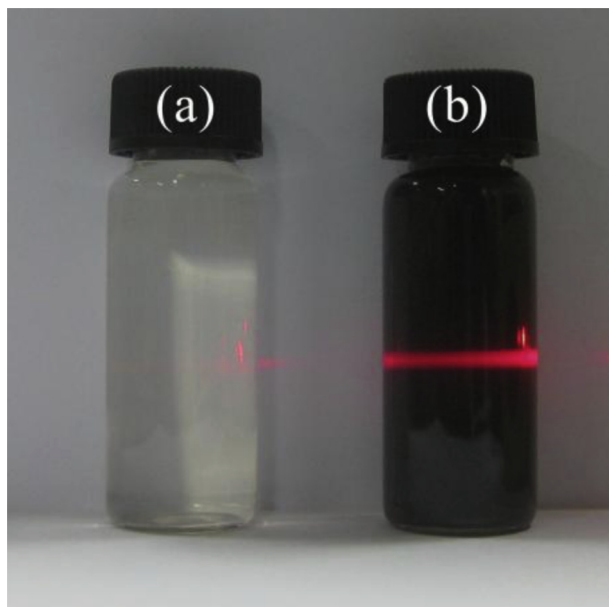


Fig. 2. Photographs of (a): GMA-GA aqueous solution (10 mg/mL), (b): Tyndall effect of GMA-GA-stabilized graphene flakes aqueous dispersion (0.1 mg/mL).

the solutions were adjusted to a value in the range of 1–12 with 0.1 M NaOH or 0.1 M HCl. The pH values were precisely checked by a pH-meter (PHS-2/Tianda, accuracy: ± 0.01).

2.7. Compressive test of hydrogel

Before compressive test, the obtained hydrogels, in its cylindrical form, were immersed in DI water for 1 week to achieve swelling equilibrium. Then, the cylindrical hydrogels were cut into pieces of 4 cm height. Using an Instron 4465 instrument, the measurement of compressive stress was performed on the cut hydrogels. The condition of compressive test was listed as follows: crosshead speed of

1 cm/min, a load cell of 2 kN, temperature of 25 °C, initial gauge length of 40 mm and final gauge length of 10 mm.

3. Results and discussion

3.1. Characterization of the exfoliated graphene flakes

GA is composed of the hydrophobic polypeptide chains and hydrophilic polysaccharides blocks [27]. It has been demonstrated that chemical modifications of GA with GMA involve epoxy ring-opening and transesterification. A schematic drawing of the reaction routes is shown in Fig. 1. The GMA-GA was successfully obtained by previously reported method [31]. FTIR, ^1H NMR analyses demonstrated the introduction of GMA in the structure of GA (Supplemental Fig. S1 and S2).

The liquid-phase direct exfoliation of graphite was carried out by sonicating the mixture aqueous dispersion of GMA-GA and pristine graphite flakes in an ice-water bath. After sonication, the GMA-GA-stabilized graphene flakes aqueous dispersion was obtained by collecting the top supernatant by centrifuging at 4000 rpm for 30 min. As shown in Fig. 2, the GMA-GA-stabilized graphene flakes aqueous dispersion is very stable and homogeneous even after one month in a sealed bottle. The colloidal nature and high stability of the graphene flakes dispersion was confirmed by the presence of Tyndall effect (Fig. 2). It indicated that graphite is exfoliated into the graphene flakes and stable colloidal graphene flakes dispersion is achieved.

TEM images were first used to characterize the exfoliated graphene flakes. Selected typical TEM images were illustrated in Fig. 3. A small quantity of few-layer graphene flakes (<4 layers) was observed in Fig. 3a. A long piece of folded graphene flake was exhibited in Fig. 3b. By paying close attention to the edges of the graphene flakes at a higher magnification, the number of layers was around 3. The cross-sectional selected area electron diffraction (SAED) pattern (inset of Fig. 3c) demonstrates the typical six-fold symmetry characteristic diffraction with an ordered well-crystallized graphene structure. In addition, a single edge-folded graphene flake of 3 layers was observed in Fig. 3d. From Fig. 3e

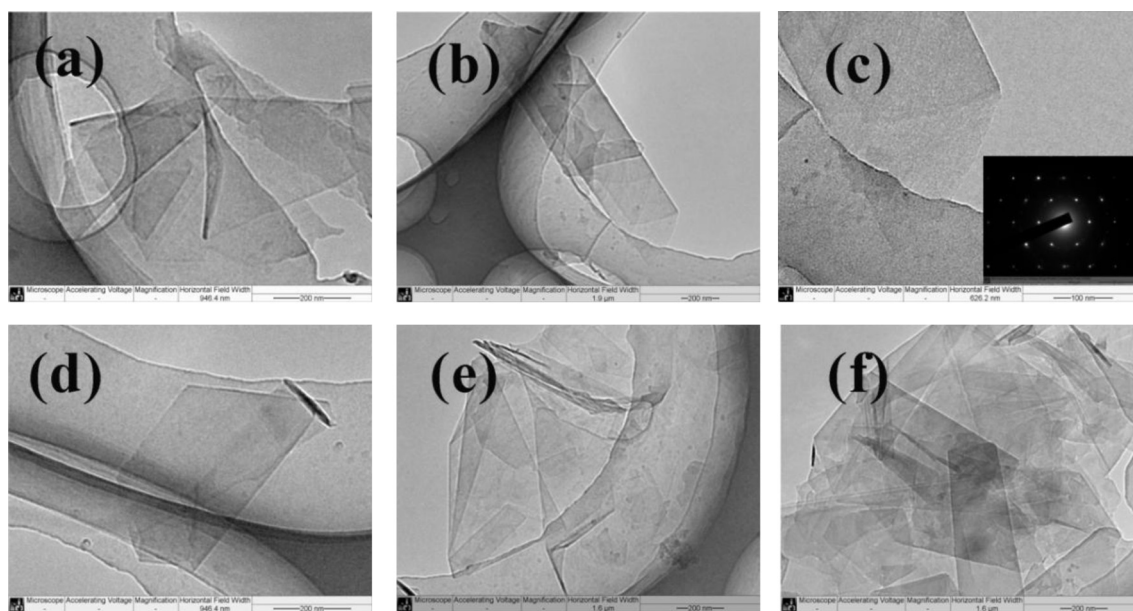


Fig. 3. Selected TEM images of graphene flakes. (a): a small quantity of stacked few-layer graphene flakes (<4 layers), (b): a long and folded graphene flake, (c): edge-on view of (b) at a higher magnification, inset of (c) shows a selected area electron diffraction (SAED) pattern, (d): a graphene flake of 3 layers with folded edge, (e) and (f): a large number of stacked and folded few-layer graphene flakes.

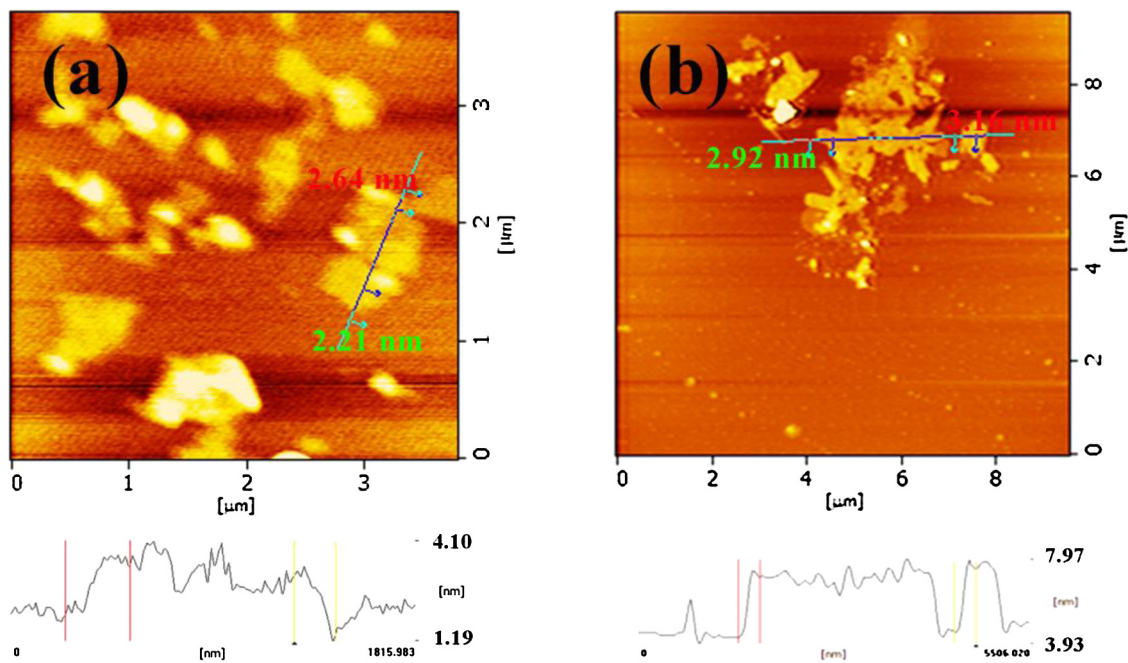


Fig. 4. AFM images of graphene flakes obtained by liquid-phase direct exfoliation with assistance of GMA-GA.

and f, there are a large number of stacked and folded few-layer graphene flakes. The TEM images demonstrated that the pristine graphite can be exfoliated into few-layer graphene flakes with assistance of GMA-GA. AFM images were also used to investigate the topography and thickness of the exfoliated graphene flakes.

The represent AFM images are shown in Fig. 4. The thicknesses of exfoliated graphene flakes were determined to be around 2.21–3.16 nm. Considering the absorbed GMA-GA which reflects the bright and white dots and intrinsic limits of AFM, the exfoliated flakes were consisted of less than 4 layers of graphene [21,23,33].

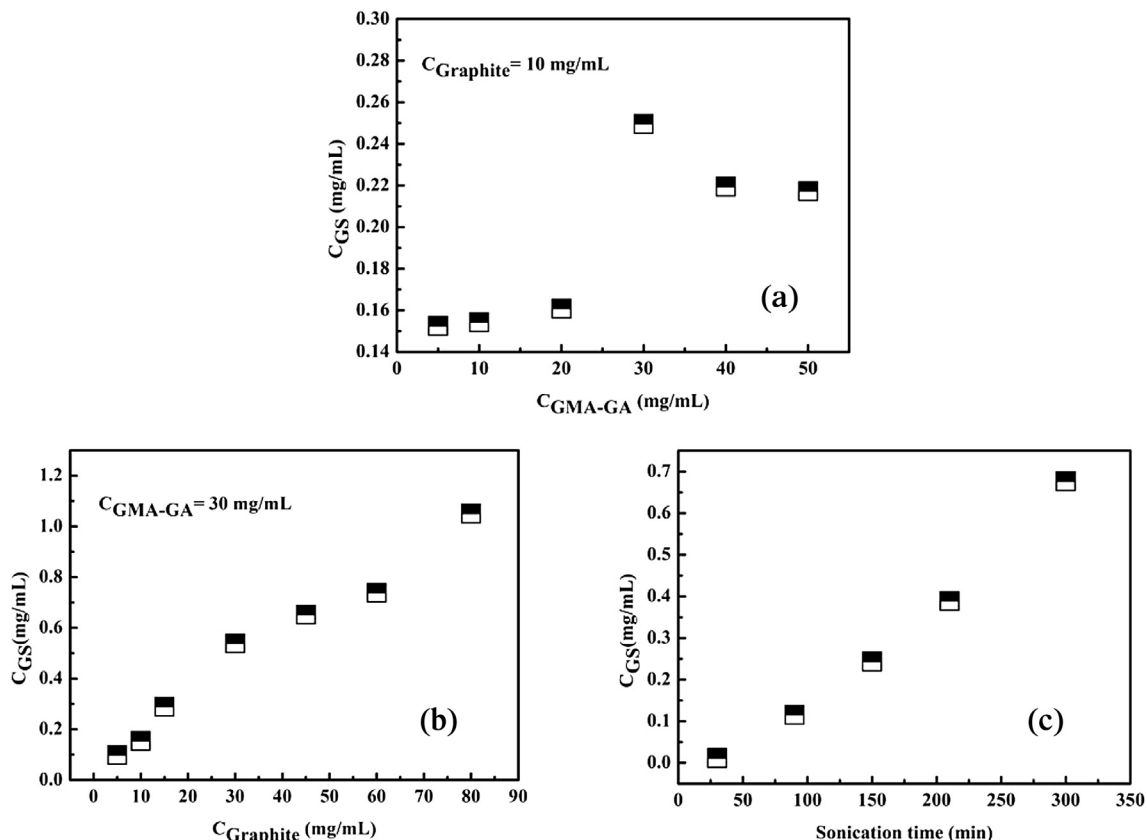


Fig. 5. Effects of (a): C_{GMA-GA} , (b): $C_{Graphite}$, and (c): sonication time on the concentration of exfoliated graphene flakes.

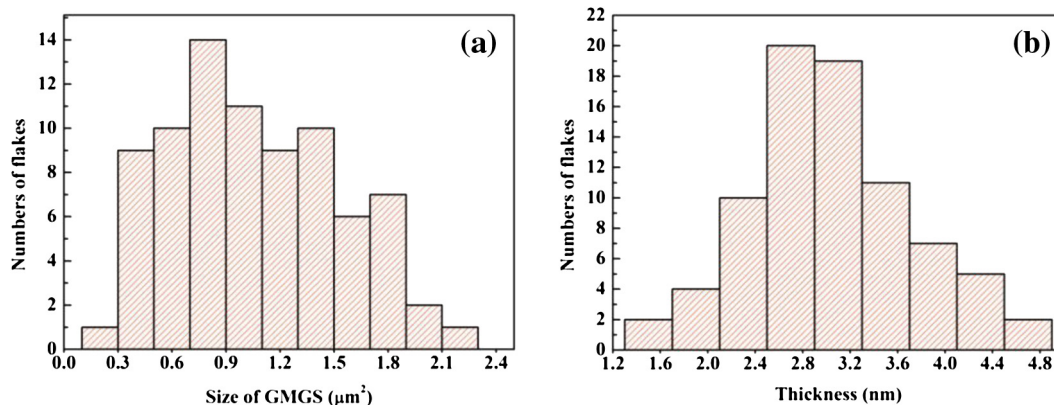


Fig. 6. The lateral dimensions (a) and thickness (b) of GMGS obtained by direct exfoliation with assist of GMA-GA.

In order to get the final concentration of GMA-GA-stabilized graphene flakes aqueous dispersion after centrifugation, the obtained dispersion was diluted and the absorption spectrum of the dispersion was recorded by UV–Vis spectrophotometry. The UV–Vis absorption spectra of GMA-GA approached zero above 500 nm (Supplemental Fig. S5). Therefore, the concentration of graphene flakes can be determined from the absorbance at 660 nm by using the extinction coefficient of graphene ($\alpha = 1390 \text{ mL mg}^{-1} \text{ m}^{-1}$) which is previously determined in surfactant/water solutions [21,25]. Using α for GMA-GA-stabilized graphene flakes aqueous dispersion, the concentration of graphene flakes (C_{GS}) can be calculated by the formula of Lambert–Beer law (Supplementary data). The efficiency of exfoliation was investigated by varying the related conditions including the initial concentration of graphite (C_{Graphite}), the concentration of GMA-GA aqueous solution ($C_{\text{GMA-GA}}$) and sonication time. As shown in Fig. 5, the C_{GS} is significantly affected by sonication time, $C_{\text{GMA-GA}}$ and C_{Graphite} . From Fig. 5a, holding the initial concentration of pristine graphite constant at 10 mg/mL, the maximum of C_{GS} achieved $\sim 0.25 \text{ mg/mL}$ after sonication of 300 min when $C_{\text{GMA-GA}}$ equals to 30 mg/mL. While the $C_{\text{GMA-GA}}$ exceeds 30 mg/mL, the C_{GS} begins to decrease. Towards to liquid-phase direct exfoliation with assistance of the surfactant, the production of graphene flakes is very close to the critical micelle concentration (CMC) of the surfactant [62,71]. The decrease of C_{GS} is attributed to the high concentration of GMA-GA which is out of CMC. Then, $C_{\text{GMA-GA}}$ was fixed at 30 mg/mL and the C_{Graphite} is changed. As is shown in Fig. 5b, the C_{GS} increased with the increase of C_{Graphite} . When C_{Graphite} reaches 80 mg/mL, the

C_{GS} increased to $\sim 1.12 \text{ mg/mL}$ (Fig. 5b) after sonication of 300 min. With the fixed $C_{\text{GMA-GA}}$ of 30 mg/mL and C_{Graphite} of 60 mg/mL, the C_{GS} increased with the sonication time. After sonication of 5 h, the C_{GS} can run up to $\sim 0.71 \text{ mg/mL}$.

To further understand the state of exfoliation of graphite, the lateral dimensions and thicknesses of exfoliated graphene flakes which were obtained after sonication of 300 min with $C_{\text{GMA-GA}}$ of 30 mg/mL and C_{Graphite} of 60 mg/mL were statistically analysed. The main distribution of size and thickness were investigated from a number of TEM and AFM images of 80 distinguishable graphene flakes (Supplemental Fig. S3 and S4). From Fig. 6, the distributions of the lateral dimensions and thicknesses were mainly concentrated at the range of 0.3–2.1 μm^2 and 1.8–4.5 nm, respectively. It demonstrated that the few-layer graphene flakes can be produced by direct exfoliation with the assistance of GMA-GA.

The exfoliation of graphite into GMGS was also demonstrated by Raman spectroscopy (Fig. 7). The Raman spectroscopy of pristine graphite is dominated by a G band at 1571 cm^{-1} and a 2D band at 2703 cm^{-1} [21,25]. After exfoliation, the obvious D-band with relative strong intensity was observed in exfoliated graphene flakes with assistance of GMA-GA. It is attributed to the edge effect from the fractions of graphene edges. Additionally, the intensity ratio of D and G band ($I_{\text{D}}/I_{\text{G}}$) reflects the structural defects and the indication of disorder [34]. Compared to reduced graphene oxide (RGO) (Fig. S6), the value of $I_{\text{D}}/I_{\text{G}}$ for GA-G is still quite lower than RGO. It indicated that the exfoliated graphene flakes exhibited low levels of defects. It is well-known that the 2D band is originated from second order-double resonant Raman scattering from zone

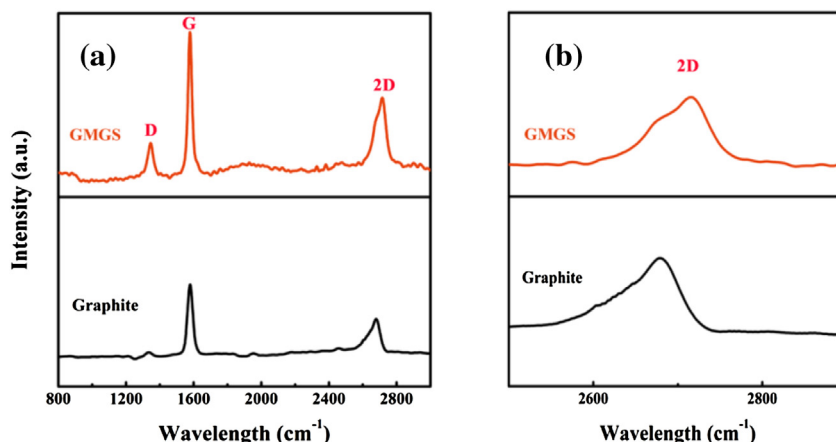


Fig. 7. (a): Raman spectroscopy of pristine graphite and GMGS, (b): Detailed 2D Raman band for GMGS and pristine graphite.

boundary. It can reflect the number of layers and can be used to distinguish single-layer, few-layer and multi-layer graphene flakes [35,36]. When the layers > 5 , the 2D-band of the graphene flakes strongly resembles the 2D-band for the pristine graphite. For the 2D band of the exfoliated graphene flakes, it is noted that the width and shape were distinguished from the pristine graphite. Therefore, we considered that the graphene and ultrathin graphite flakes can be obtained by direct exfoliation with assist of GMA-GA. The result is consistent with TEM and AFM measurements.

Similar to surfactant-stabilized graphene flakes dispersion by direct exfoliation, GMA-GA is expected to adsorb onto the exfoliated graphene flakes. It is expected that the electrostatic repulsion between GMA-GA and graphene flakes facilitated the stabilization of graphene flakes. Zeta potentials were used to characterize the dispersions [21]. As is shown in Fig. 8, it is observed the distribution of zeta potentials for pristine graphite aqueous dispersion centred at 11.8 mV (Fig. 8a). The zeta potential of GMA-GA aqueous solution (10 mg/mL) was centred at -19.9 mV. For GMA-GA-stabilized graphene flakes dispersion (0.5 mg/mL), the zeta potential peak for colloidal stability of -12.1 mV, fall in between the pristine graphite and GMA-GA aqueous solution. It indicated that there is electrostatic interaction between the GMA-GA and graphene flakes. The pH value of GMGS aqueous dispersion was varied by addition of 0.1 M HCl and NaOH water solution. As the pH value increased, there is a trend toward more negative zeta potential values due to the increase of negative OH^- charges (Fig. 8b). After exfoliation, the GMA-GA coated on the surface of exfoliated graphene flakes facilitated the dispersion of GMGS.

GMGS can be considered as hybrids of GMA-GA and exfoliated graphene flakes. FTIR spectra were used to characterize the introduction of GMA-GA. As is shown in Fig. 9a, the peak at 3410 cm^{-1} was characteristic peak of hydroxyl groups of polysaccharides blocks from GMA-GA. The peak at 1716 cm^{-1} was attributed to the

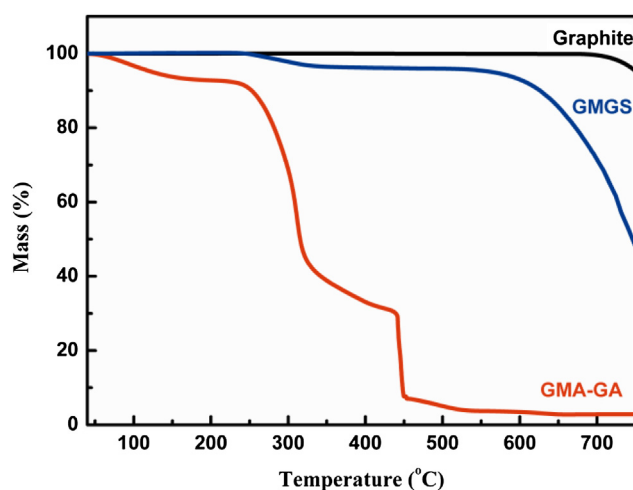


Fig. 10. TGA curves of graphite, GMA-GA and GMGS.

$\text{C}=\text{O}$ stretching vibration of conjugated ester groups. The $\text{C}=\text{C}$ stretching frequency was observed at 1637 cm^{-1} in the spectra of GMGS [31]. The vinyl groups coming from GMA-GA were coupled into the polysaccharide chains of GA. The results demonstrated the introduction of GMA-GA in GMGS. The XRD patterns were also used to characterize the GMGS. In Fig. 9b, for pristine graphite, the diffraction peak at 26.2° is attributed to the (002) reflection of a hexagonal graphite structure [37,38]. After exfoliation, the diffraction peak at 26.2° still exists in the filtration film of GMGS. It is indicated that the GMGS were restack to form graphite-like structure in the film preparation process. For GMGS, it's worth noting that there is an evident broaden peak around 23° . It is attributed to

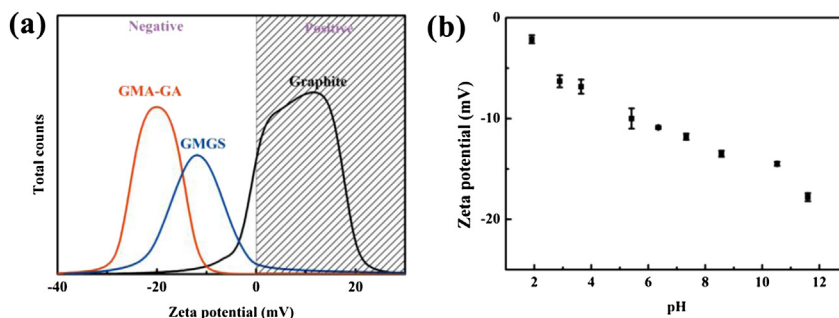


Fig. 8. (a): Zeta potentials of GMA-GA water solution (0.5 mg/mL), GMGS aqueous dispersion (0.2 mg/mL) and pristine graphite aqueous dispersion (0.2 mg/mL), (b): Zeta potentials of GMGS aqueous dispersions with different pH values.

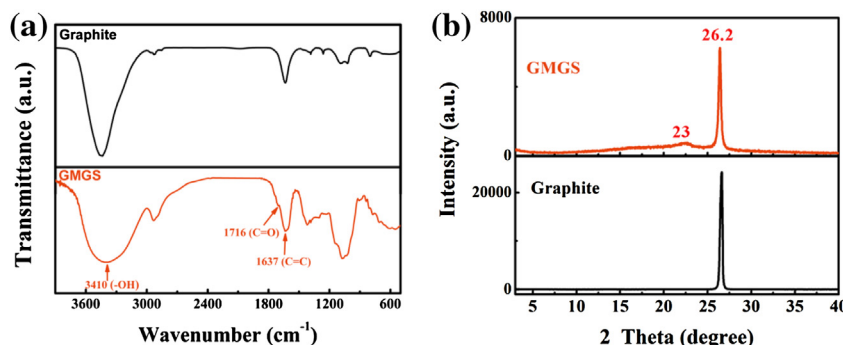


Fig. 9. (a): FTIR spectra of pristine graphite and GMGS, (b): XRD patterns of pristine graphite and GMGS.

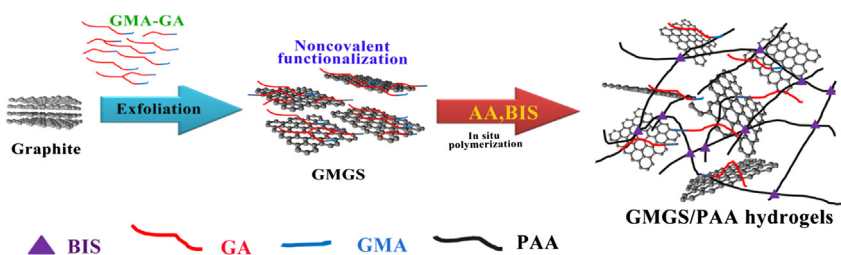


Fig. 11. Illustration of the process for preparation of GMGS-PAA hydrogels by *in situ* polymerization.

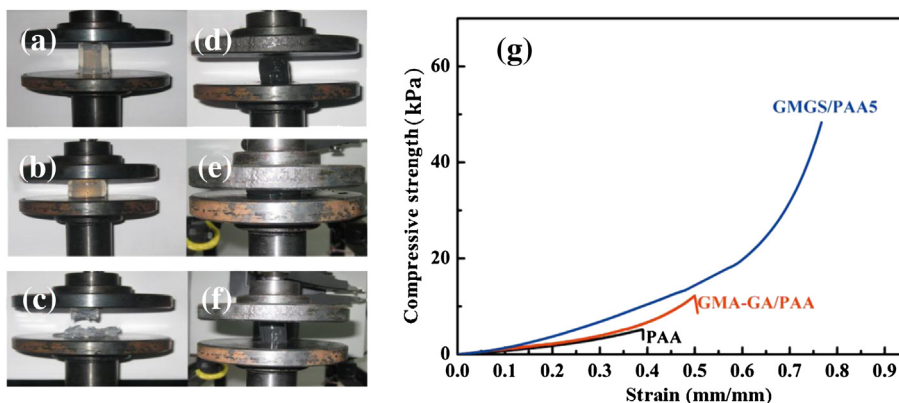


Fig. 12. Photographs of GMA-GA/PAA hydrogel ((a), (b) and (c)) and GMGS/PAA5 hydrogel ((d), (e) and (f)) under different state of compression, (g): The typical compressive stress–strain curves for PAA hydrogel, GMA-GA/PAA hydrogel and GMGS/PAA5 hydrogel.

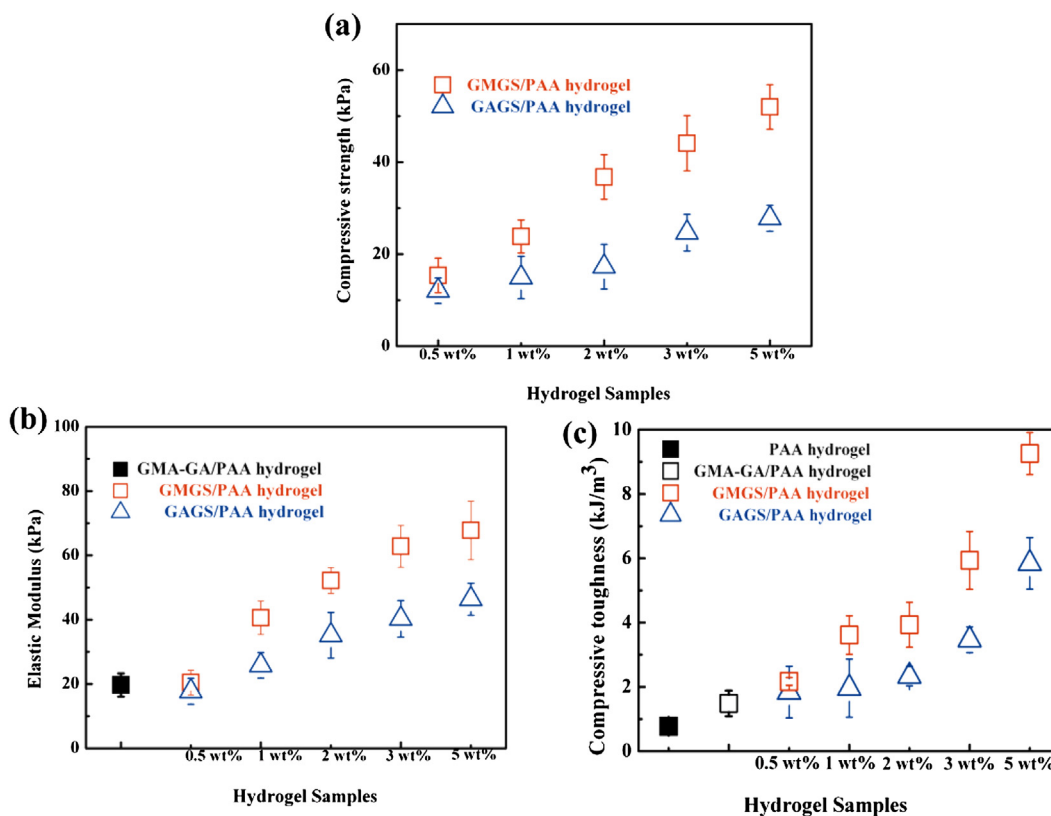


Fig. 13. (a): Compressive strengths of GMGS/PAA, GAGS/PAA hydrogels with various fillers weight fractions, (b): Compressive elastic modulus of GMA-GA/PAA hydrogel, GMGS/PAA and GAGS/PAA hydrogels with various fillers weight fractions, and (c) Compressive toughness of PAA hydrogel, GMA-GA/PAA hydrogel, GMGS/PAA and GAGS/PAA hydrogels with various fillers weight fraction.

the amorphous structure of GMA-GA in the GMGS. TGA analysis was performed for determining the components ratio of GMA-GA in GMGS. From Fig. 10, pristine graphite shows an evident degradation at temperature higher than 700 °C [39]. Judging from the weight loss at the plateau region around 750 °C, the amount of GMA-GA accounts for ~48.7 wt% in the GMGS.

3.2. Fabrication of GMGS/PAA composite hydrogel

The GMGS/PAA hydrogel were fabricated by *in situ* polymerization of AA in presence of GMGS. As is shown in Fig. 11, the vinyl groups, originated from the GMA-GA in GMGS, can provide the grafting points in hydrogel formation. Therefore, GMGS, leading to the grafting of PAA chains onto the exfoliated graphene flakes, could act as a multifunctional cross-linker in polymerization for improving the mechanical properties of the hydrogel.

By changing the amount of GMGS, the GMGS/PAA0.5, GMGS/PAA1, GMGS/PAA2, GMGS/PAA3 and GMGS/PAA5 hydrogels were prepared by *in situ* polymerization. In the meantime, according to the previous TGA analysis, there is ~48.7 wt% of GMA-GA in the composition of GMGS. Therefore, the GMA-GA/PAA hydrogel with ~2.5 wt% of GMA-GA was also prepared for comparison. The compressive tests were performed for evaluating the mechanical properties of the hydrogels. The typical compressive stress–strain curves for PAA, GMA-GA/PAA and GMGS/PAA5 hydrogels were illustrated in Fig. 12g. The PAA and GMA-GA/PAA hydrogels were broken till the compressive strength reach ~5.2 and ~12.3 kPa, respectively. However, there is no break for GMGS/PAA5 hydrogel even at the compressive strength of ~49.2 kPa. From Fig. 12a–f, the photographs of compressive tests of the GMA-GA/PAA and GMGS/PAA5 hydrogel, the GMGS/PAA5 can recover its original cylinder shape after compression. The phenomenon offers the direct information of improvement in mechanical properties after introduction of GMGS in the network of PAA hydrogel.

GA itself can be used for liquid-phase direct exfoliation of graphite. With liquid-phase direct exfoliation, the GAGS were also collected by centrifugalization. The GAGS/PAA hydrogels with different amount of GAGS were also prepared by *in situ* polymerization. The compressive strengths, elastic modulus and toughness of GMGS/PAA and GAGS/PAA hydrogels were illustrated in Fig. 13a and b. The compressive strength of PAA hydrogels is ~5.2 kPa. After introduction of GMGS and GAGS, the mechanical properties of the hydrogels were both improved. The compressive strengths of GMGS/PAA, GAGS/PAA hydrogels increased with the loading of GMGS and GAGS. When the loading amount reached 5 wt%, the compressive strengths of GAGS/PAA, GMGS/PAA5 hydrogels arrived at ~29.1 and ~51.9 kPa. From Fig. 12, the mechanical property of GMA-GA/PAA hydrogel was also improved compared to PAA hydrogel. After introduction of GMA-GA, the GMA-GA/PAA

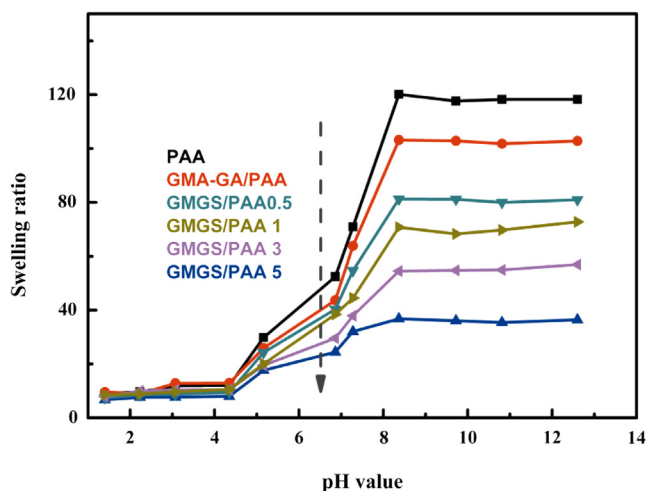


Fig. 15. The SR of PAA and GMGS/PAA hydrogels in different pH values at room temperature.

hydrogel was formed by *in situ* copolymerization cross-linked by BIS. The GMA-GA polymer chains were chemically linked to the PAA chains in the networks of GMA-GA/PAA hydrogel [31]. Meantime, there are interactions between the GMA-GA and PAA chains. These are contributed to the improvement of mechanical properties. Towards for the GAGS/PAA hydrogels, the mechanical properties of composite hydrogels were improved with incorporation with GAGS. It is generally known that GA is composed of a highly branched arrangement of the simple sugars galactose, arabinose, rhamnose, and glucuronic acids and also contains a protein component covalently bound within its molecular arrangement [27]. In the networks of GAGS/PAA hydrogels, there are strong hydrogen bonds between the functional groups of GA and –COOH groups of PAA chains. Successively, the inserted GAGS in the three-dimensional networks hindered the shape change of hydrogel in the compression with the strong interaction of PAA chain and GAGS. By contrast, it is worth noting that the compressive strengths and the elastic modulus of GMGS/PAA were both superior to the GAGS/PAA hydrogels obviously. The elastic modulus of hydrogel was determined according to the slope of compressive stress–strain curves above 50% of compressive deformation. The compressive strength and elastic modulus of GMGS/PAA5 hydrogel reach ~49.2 and ~66.9 kPa, which are increases of ~306.6% and ~251.6% compared to GMA-GA/PAA hydrogel. In the meantime, the compressive toughness was also calculated for further understanding the improvement of mechanical property. From Fig. 13c, the compressive toughness of PAA and GMA-GA/PAA

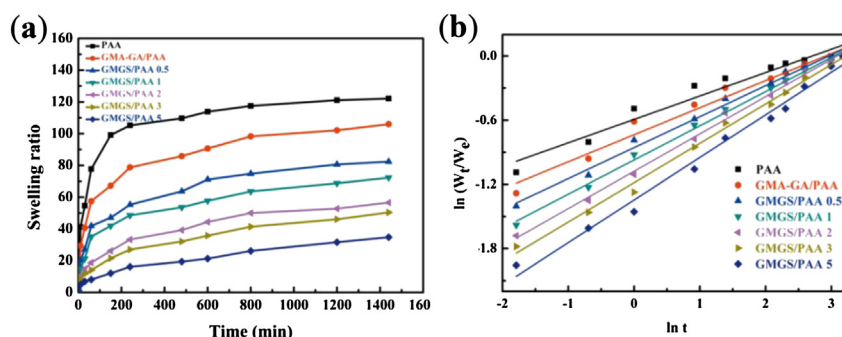


Fig. 14. (a): Swelling kinetics of PAA, GMA-GA/PAA and GMGS/PAA hydrogels, (b): $\ln(W_t/W_0)$ versus $\ln t$ for PAA, GMA-GA/PAA and GMGS/PAA hydrogels.

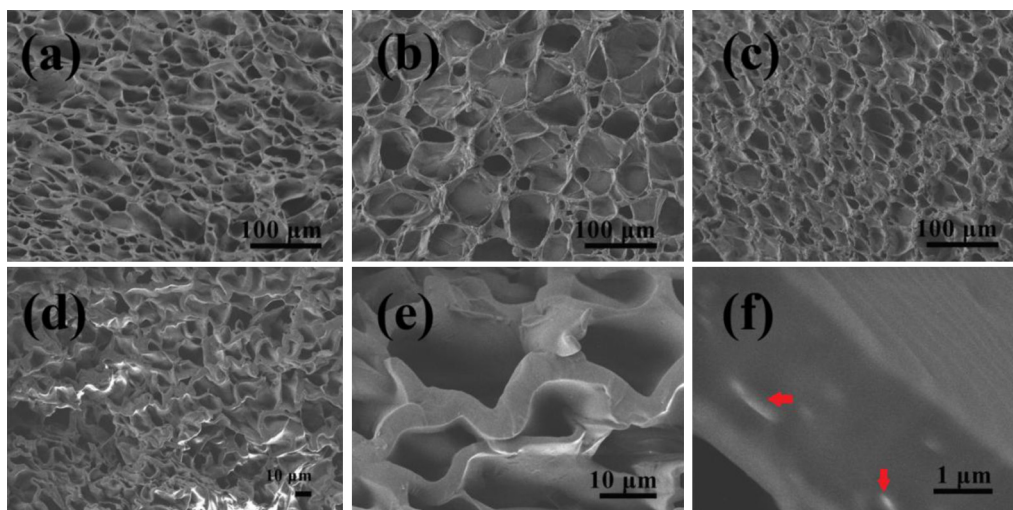


Fig. 16. SEM images of (a): PAA, (b): GMA-GA/PAA, (c): GMGS/PAA3 and (d): GMGS/PAA5 hydrogels; (e and f): a partial enlarged view of (d) with different magnification.

hydrogels were around 1.48 and ~ 1.83 kJ/m³, accompany with the break at the relatively low compressive deformation. Obviously, the compressive toughness of GMGS/PAA5 hydrogel reaches ~ 9.2 kJ/m³, which is higher than the GAGS/PAA5 hydrogel (~ 5.8 kJ/m³). Such evident improvement in compressive strength, elastic modulus and toughness is most likely caused by the dual function of cross-link of copolymerization and interaction between GMGS and PAA chain. Additionally, the compressive strength, elastic modulus and toughness were increased with the amount of GMGS. The presence of GMGS chains inside of the hydrogel makes the networks of the hydrogel denser and enhanced the mechanical property of the hydrogel.

The SR was also used to characterize the hydrogel. Fig. 14 shows the SR of the hydrogels as a function of time in DI water at room temperature. As is well-known, the water up-take process of hydrogels is corresponded to the diffusion of water into the hydrogel network. For investigating the diffusion model for swelling of the hydrogel, the swelling data was fitted to the exponential heuristic equation:

$$W_t/W_e = kt^n,$$

where W_t is the weight of the hydrogel at a given time during swelling process, W_e is the weight of the equilibrium swollen hydrogel, t is the time of swelling, k is the characteristic constant of hydrogel, and n is the characteristic exponent, which is related to the transport mode of penetrate. When $n = 0.5$, the transport mode of penetration fits the Fickian diffusion law. In cases, where $0.5 < n < 1$, they are generally considered as anomalous diffusion [11,40]. The fit line of $\ln(W_t/W_e)$ versus $\ln t$ for PAA, GMA-GA/PAA and GMGS/PAA hydrogels were illustrated in Fig. 14b. The value of n can be determined with the slope of the fit line. For the PAA hydrogel, the value of n is 0.46. While for GMGS/PAA composite hydrogel, the value of n increased from 0.508 for GMGS/PAA0.5 to 0.67 for GMGS/PAA5. It suggested an apparently non-Fickian anomalous diffusion occurs with increase of GMGS. Additionally, the GMGS/PAA composite hydrogel shows pH-sensitive swelling behaviour. From Fig. 15, it can be seen that the SR of the composite hydrogel was related to the pH value. With $\text{pH} < 5$, the composite hydrogel is not fit for absorbing water. When the $\text{pH} > 5$, the SR begin to increase greatly. For the GMGS/PAA composite hydrogel, there are carboxylic acid groups in the glucuronic acid segments of GMGS and PAA chains. When $\text{pH} > 5$, the hydrogen bond broke as carboxylic acid groups ionized, and at the same time,

electrostatic repulsion caused the network to expand, the SR of hydrogel increased sharply [41,42].

In the meantime, the SR decreased with the increased amount of GMGS in GMGS/PAA composite hydrogels. The mechanical properties and SR of hydrogels is related to the cross-linking density [43]. Since the GMGS will have strong hydrogen bonding effect with PAA, these GMGS will “increase” the cross-linking densities. It is more important that the GMGS can cross-link to the PAA chains in the networks of hydrogel. Due to the higher cross-linking densities, the mobility of polymer chains in the networks was restricted. On the other hand, the interspersed layered GMGS in the hydrogel networks further hindered the movement of polymer chains of hydrogel. Thus, the SR of GMGS/PAA hydrogel decreased with the volume fractions of GMGS. The mechanical properties of hydrogels were greatly improved with hybridization of GMGS and PAA. SEM images were characterized the morphology of hydrogel. As is shown in Fig. 16, it can be clearly seen that the hydrogel samples shows sponge-like architecture with pore diameters at micrometric level. From the SEM images, the holes of hydrogel are uniformly distributed in large scale. From the SEM images of GMGS/PAA hydrogel (Fig. 16c and d), the network structure of hydrogel becomes thicker and denser. The layered structure of GMGS can be observed in high resolution as pointed by red arrows in Fig. 16f. It implied that the compressive deformation of GMGS/PAA hydrogel of needs more energy compared to PAA hydrogel.

4. Conclusion

GMA-GA was obtained by chemically modification of GA with GMA in aqueous/DMSO solution. Through two different pathway reactions, epoxy ring-opening and transesterification, the vinyl groups of C=C coming from GMA were coupled onto the polysaccharide structure of GA. After modification, the GMA-GA can still be used for liquid-phase direct exfoliation of graphite. With assist of GMA-GA, the maximum concentration of graphene flakes can reach ~ 1.12 mg/mL. The GMGS were introduced into a PAA hydrogel to improve its mechanical property. The compressive tests were performed for determining the mechanical properties of hydrogels. The compressive strength and elastic modulus of GMGS/PAA5 composite hydrogel reach ~ 49.2 and ~ 66.9 kPa, which are increases of ~ 846.1 and $\sim 243.7\%$ compared to PAA hydrogel. The results demonstrated that the GMGS are superior to the GMA-GA and GAGS in mechanical reinforcement of hydrogel.

Acknowledgements

We acknowledge the supports from National Nature Science Foundation of China (No. 50973062). We are grateful to researchers in the instrument analysis center of Shanghai Jiao Tong University for their help in material analysis.

Appendix A. Supplementary data

Supplementary data related to this article can be found at <http://dx.doi.org/10.1016/j.polymer.2013.05.057>.

References

- [1] Wu Y, Xia M, Fan Q, Zhu M. *Chemical Communications* 2010;46(41):7790–2.
- [2] Qiu Y, Park K. *Advanced Drug Delivery Reviews* 2001;53(3):321–39.
- [3] Hoffman AS. *Advanced Drug Delivery Reviews* 2012;64(Suppl. (0)):18–23.
- [4] Sun J-Y, Zhao X, Illeperuma WRK, Chaudhuri O, Oh KH, Mooney DJ, et al. *Nature* 2012;489(7414):133–6.
- [5] Gong JP, Katsuyama Y, Kurokawa T, Osada Y. *Advanced Materials* 2003;15(14):1155–8.
- [6] Geim AK, Novoselov KS. *Nature Materials* 2007;6(3):183–91.
- [7] Das S, Wajid AS, Shelburne JL, Liao Y-C, Green MJ. *ACS Applied Materials & Interfaces* 2011;3(6):1844–51.
- [8] Potts JR, Dreyer DR, Bielawski CW, Ruoff RS. *Polymer* 2011;52(1):5–25.
- [9] Dreyer DR, Park S, Bielawski CW, Ruoff RS. *Chemical Society Reviews* 2010;39(1):228–40.
- [10] Dikin DA, Stankovich S, Zimney EJ, Piner RD, Dommett GHB, Evmenenko G, et al. *Nature* 2007;448(7152):457–60.
- [11] Shen J, Yan B, Li T, Long Y, Li N, Ye M. *Soft Matter* 2012;8(6):1831–6.
- [12] Liu R, Liang S, Tang X-Z, Yan D, Li X, Yu Z-Z. *Journal of Materials Chemistry* 2012;22(28):14160–7.
- [13] Coleman JN. *Accounts of Chemical Research* 2013;46(1):14–22.
- [14] Lotya M, King PJ, Khan U, De S, Coleman JN. *ACS Nano* 2010;4(6):3155–62.
- [15] Schniepp HC, Kudin KN, Li J-L, Prud'homme RK, Car R, Saville DA, et al. *ACS Nano* 2008;2(12):2577–84.
- [16] Su Q, Pang S, Aljani V, Li C, Feng X, Müllen K. *Advanced Materials* 2009;21(31):3191–5.
- [17] Kim H, Macosko CW. *Macromolecules* 2008;41(9):3317–27.
- [18] May P, Khan U, O'Neill A, Coleman JN. *Journal of Materials Chemistry* 2012;22(4):1278–82.
- [19] Khan U, O'Neill A, Porwal H, May P, Nawaz K, Coleman JN. *Carbon* 2012;50(2):470–5.
- [20] Hernandez Y, Nicolosi V, Lotya M, Blighe FM, Sun Z, De S, et al. *Nature Nanotechnology* 2008;3(9):563–8.
- [21] Lotya M, Hernandez Y, King PJ, Smith RJ, Nicolosi V, Karlsson LS, et al. *Journal of the American Chemical Society* 2009;131(10):3611–20.
- [22] Wang Y, Shi Z, Fang J, Xu H, Ma X, Yin J. *Journal of Materials Chemistry* 2011;21(2):505–12.
- [23] Vadukumpully S, Paul J, Valiyaveetil S. *Carbon* 2009;47(14):3288–94.
- [24] Das S, Irin F, Tanvir Ahmed HS, Cortinas AB, Wajid AS, Parviz D, et al. *Polymer* 2012;53(12):2485–94.
- [25] Guardia L, Fernández-Merino MJ, Paredes JI, Solís-Fernández P, Villar-Rodil S, Martínez-Alonso A, et al. *Carbon* 2011;49(5):1653–62.
- [26] Liu F, Choi JY, Seo TS. *Chemical Communications* 2010;46(16):2844–6.
- [27] Islam AM, Phillips GO, Sljivo A, Snowden MJ, Williams PA. *Food Hydrocolloids* 1997;11(4):493–505.
- [28] Lu E-X, Jiang Z-Q, Zhang Q-Z, Jiang X-G. *Journal of Controlled Release* 2003;92(3):375–82.
- [29] Fan J, Shi Z, Ge Y, Wang J, Wang Y, Yin J. *Journal of Materials Chemistry* 2012;22(27):13764–72.
- [30] Zohuriaan-Mehr MJ, Motazedi Z, Kabiri K, Ershad-Langroudi A, Allahdadi I. *Journal of Applied Polymer Science* 2006;102(6):5667–74.
- [31] Reis AV, Guilherme MR, Cavalcanti OA, Rubira AF, Muniz EC. *Polymer* 2006;47(6):2023–9.
- [32] Brannon-Peppas L, Peppas NA. *Chemical Engineering Science* 1991;46(3):715–22.
- [33] Reina A, Jia X, Ho J, Nezich D, Son H, Bulovic V, et al. *Nano Letters* 2008;9(1):30–5.
- [34] Shao G, Lu Y, Wu F, Yang C, Zeng F, Wu Q. *Journal of Materials Science* 2012;47(10):4400–9.
- [35] Graf D, Molitor F, Ensslin K, Stampfer C, Jungen A, Hierold C, et al. *Nano Letters* 2007;7(2):238–42.
- [36] Ferrari AC, Meyer JC, Scardaci V, Casiraghi C, Lazzeri M, Mauri F, et al. *Physical Review Letters* 2006;97(18):187401.
- [37] Becerril HA, Mao J, Liu Z, Stoltenberg RM, Bao Z, Chen Y. *ACS Nano* 2008;2(3):463–70.
- [38] Lu W, Liu S, Qin X, Wang L, Tian J, Luo Y, et al. *Journal of Materials Chemistry* 2012;22(18):8775–7.
- [39] Jeon I-Y, Choi H-J, Bae S-Y, Chang DW, Baek J-B. *Journal of Materials Chemistry* 2011;21(21):7820–6.
- [40] Xiang Y, Peng Z, Chen D. *European Polymer Journal* 2006;42(9):2125–32.
- [41] Li X, Wu W, Wang J, Duan Y. *Carbohydrate Polymers* 2006;66(4):473–9.
- [42] Zhang X-Z, Yang Y-Y, Wang F-J, Chung T-S. *Langmuir* 2002;18(6):2013–8.
- [43] Brøndsted H, Kopeček Ji. *Biomaterials* 1991;12(6):584–92.